Pulsed Laser Deposition and Processing of Wide Band Gap Semiconductors and Related Materials

R.D. VISPUTE,[1,2,3] S. CHOOPUN,[1] R. ENCK,[1] A. PATEL,[1] V. TALYANSKY,[1] R.P. SHARMA,[1] T. VENKATESAN,[1] W.L. SARNEY,[2] L. SALAMANCA-RIBA,[2] S.N. ANDRONESCU,[4] A.A. ILIADIS,[4] and K.A. JONES[5]

1.—CSR, Department of Physics, University of Maryland, College Park, MD 20742. 2.—Department of Materials and Nuclear Engineering, University of Maryland, College Park, MD 20742. 3.—e-mail: Vispute@squid.umd.edu. 4.—Department of Electrical Engineering, University of Maryland, College Park, MD 20742. 5.—Army Research Laboratory, AMSRL-PS-DS, Fort Monmouth, NJ 07703

The present work describes the novel, relatively simple, and efficient technique of pulsed laser deposition for rapid prototyping of thin films and multi-layer heterostructures of wide band gap semiconductors and related materials. In this method, a KrF pulsed excimer laser is used for ablation of polycrystalline, stoichiometric targets of wide band gap materials. Upon laser absorption by the target surface, a strong plasma plume is produced which then condenses onto the substrate, kept at a suitable distance from the target surface. We have optimized the processing parameters such as laser fluence, substrate temperature, background gas pressure, target to substrate distance, and pulse repetition rate for the growth of high quality crystalline thin films and heterostructures. The films have been characterized by x-ray diffraction, Rutherford backscattering and ion channeling spectrometry, high resolution transmission electron microscopy, atomic force microscopy, ultraviolet (UV)-visible spectroscopy, cathodoluminescence, and electrical transport measurements. We show that high quality AlN and GaN thin films can be grown by pulsed laser deposition at relatively lower substrate temperatures (750–800°C) than those employed in metalorganic chemical vapor deposition (MOCVD), (1000–1100°C), an alternative growth method. The pulsed laser deposited GaN films (~0.5 μm thick), grown on AlN buffered sapphire (0001), shows an x-ray diffraction rocking curve full width at half maximum (FWHM) of 5–7 arc-min. The ion channeling minimum yield in the surface region for AlN and GaN is ~3%, indicating a high degree of crystallinity. The optical band gap for AlN and GaN is found to be 6.2 and 3.4 eV, respectively. These epitaxial films are shiny, and the surface root mean square roughness is ~5–15 nm. The electrical resistivity of the GaN films is in the range of 10^{-2}–10^{2} Ω-cm with a mobility in excess of 80 $cm^2V^{-1}s^{-1}$ and a carrier concentration of 10^{17}–10^{19} cm^{-3}, depending upon the buffer layers and growth conditions. We have also demonstrated the application of the pulsed laser deposition technique for integration of technologically important materials with the III-V nitrides. The examples include pulsed laser deposition of ZnO/GaN heterostructures for UV-blue lasers and epitaxial growth of TiN on GaN and SiC for low resistance ohmic contact metallization. Employing the pulsed laser, we also demonstrate a dry etching process for GaN and AlN films.

Key words: AlN, deposition epitaxy, GaN, pulsed-laser

INTRODUCTION

Wide band gap semiconductors such as III-V nitrides and SiC have now been recognized as potential materials for the generation of optoelectronic devices and high temperature-high power devices.[1] However, the success of utilizing the full potential of these materials, particularly Ga-Al-In-N based systems, has not been fully realized due to the the lack of high quality lattice matched substrates, and the subse-

(Received August 1, 1998; accepted December 15, 1998)

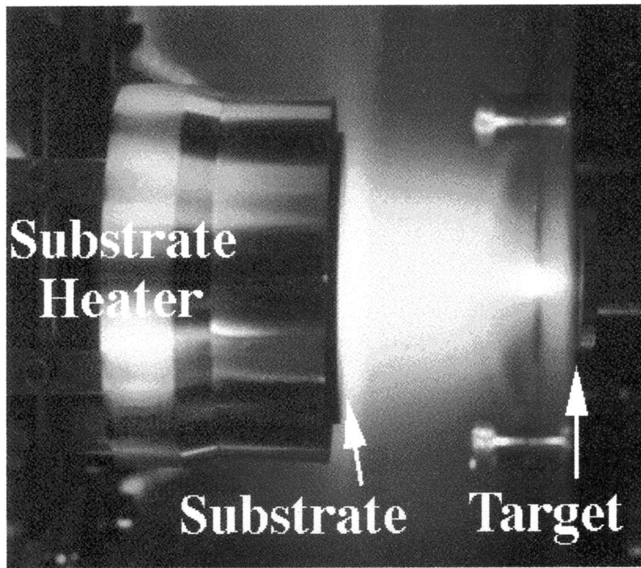

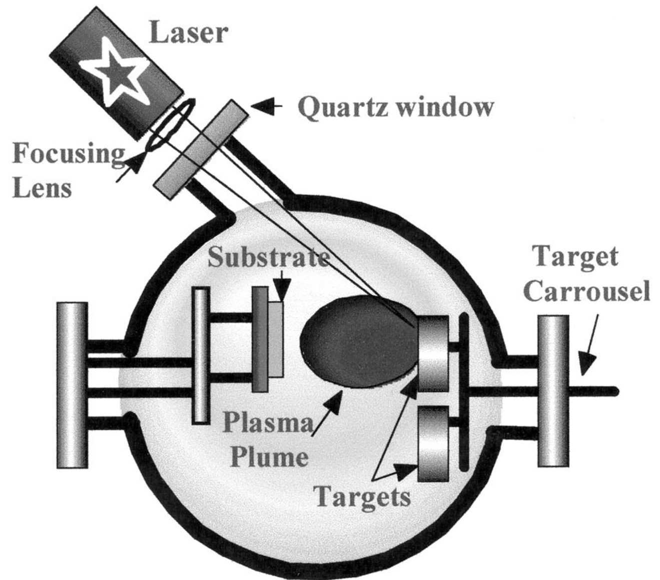

Fig. 1. Schematic of the pulsed laser deposition system (on the right) and the photograph of the pulsed laser induced plasma plume (on the left) taken during pulsed laser deposition process.

quent high defect density in the epilayers grown on them, the presence of a large intrinsic donor concentration, a difficulty in controlling electronic properties, and the lack of a suitable etchant. Thus, current research has been directed toward the fabrication of lattice matched substrates and the subsequent growth of high quality thin films with low dislocation densities (10^4–10^5/cm^2), controlled p and n-type doping, dopant activation, phase segregation, and etching processes for the fabrication of devices.[2]

In the last few years, significant progress has been made in each of the areas listed above. However, two problems still persist: 1) the lack of a lattice matched substrate for GaN epitaxy, and 2) the high growth temperature. Despite its poor structural and thermal match to GaN, sapphire has been the substrate material of choice due to its low cost, availability in large area wafers, and its high optical transparency in the ultraviolet (UV)-visible region. However, as-grown nitride films on sapphire are known to contain a high density of defects (mainly threading dislocations),[3] which affect both the electrical and optical properties of the devices. Due to the large lattice mismatch and the large interface energy between GaN and sapphire, GaN tends to grow three-dimensionally (3D) rather than layer by layer (2D). It has been shown that 3D growth can be effectively suppressed, and the crystallinity as well as surface quality can be improved, by using a two-step growth process which utilizes a buffer layer such as AlN, or lower temperature grown GaN.[4,5] In general, thicker GaN layers are grown to achieve lower dislocation densities near the surface region. The other approach followed recently by several workers is the epitaxial lateral over growth (ELOG) of GaN,[6] which resulted in a significant reduction of the dislocation densities in the GaN films that improved the life of the blue lasers.[7]

Most of the GaN researchers so far have employed growth techniques based on chemical vapor deposition (low pressure and atmospheric pressure metalorganic chemical vapor deposition (MOCVD),[8,9] atomic layer epitaxy (ALE),[10,11] vapor phase epitaxy (VPE)),[12,13] and molecular beam epitaxy (N_2 plasma assisted or NH_3 reactive molecular beam epitaxy).[14,15] In CVD, the gases such as TMG, TMA, and TMI react with NH_3 at a substrate temperature of 1050°C. A disadvantage of the CVD approach is the substantially high growth temperatures necessary to thermally dissociate NH_3 to form the desired nitride phase. The high temperature growth process introduces thermal strain and defects in the epilayers on account of the large thermal mismatch between the substrate and the film. In addition, the high thermal budget also introduces undesirable effects such as phase segregation, dopant desorption, chemical reactions at the interface, and substrate surface deterioriation.

To circumvent the high temperature growth, many groups explored the molecular beam epitaxy (MBE) technique for III-V nitrides. However, the major impediment in the physical vapor deposition (PVD) of GaN is the inertness of both N_2 and Ga species. The N_2 molecule is strongly bonded (9.5 eV), and thus it is difficult to break up for incorporation of the nitrogen into a growing film.[17] To break this bond and activate the nitrogen species, a plasma enhanced source or electron cyclotron resonance source (ECR)[14] is generally employed. Another approach using NH_3 as a reactive gas in MBE has now been successfully demonstrated.[15–17]

We recently have reported on the novel physical vapor deposition technique, pulsed laser deposition (PLD),[19,20] for the growth of epitaxial III-V nitrides. In the past, this technique has been extensively employed for the preparation of high quality thin films of multi-component metal-oxide ceramics.[21] The desirable features of PLD are:

- A non-equilibrium evaporation process which

produces an intense plasma plume and transfers the target composition (particularly metallic constituents in the multi-component systems) into the deposited film,

- The atomic-layer control achieved by adjusting the laser fluence and pulse rate, and
- An *in-situ* processing of multi-layer heterostructures by using a multiple target carousel.

This provides a unique opportunity to study the growth of GaN on various PLD grown, lattice matched, oxide buffer layers (ZnO, $LiAlO_2$, $LiGaO_2$, $ScAlMgO_4$) on sapphire in order to reduce the dislocation density in the GaN films. We have also reported on the growth of high quality epitaxial ZnO films on sapphire by PLD for heteroepitaxy with GaN.[22] Therefore, GaN/ZnO multilayer heterostructures can be fabricated via an entirely *in-situ* process by using GaN and ZnO targets. Using the PLD technique, Vispute et al. have demonstrated high quality epitaxial growth of AlN films on sapphire,[23] and Xiao et al. have reported on textured GaN films (by liquid target PLD) on fused silica.[24] Epitaxial $Al_xGa_{1-x}N$ thin films have also been reported by Huang et al. using the PLD technique.[25] In this paper, we report recent advances in the PLD of GaN and AlN, TiN metallization of GaN and SiC, and ZnO/GaN heterostructures. We discuss issues of growth, interfaces, surface morphology, structural, optical, and transport properties, and the integration of III-V nitrides with metal oxides for future generation of novel devices.

EXPERIMENTAL

Pulsed Laser Deposition

The schematic for PLD is shown in Fig. 1. A stainless steel vacuum chamber was evacuated by turbomoleculer pump to a base pressure of 7×10^{-8} Torr. A KrF excimer laser ($\lambda = 248$ nm, $\tau = 25$ ns) was used for ablation of polycrystalline, stoichiometric AlN and GaN targets (99.99 purity) at an energy density of ~1 J/cm^2. A strong absorption of the 248 nm laser radiation by the target produced an intense plasma plume in front of the target surface upon laser irradiation. The ablated material was then deposited onto the substrates kept at a suitable distance from the target surface. The NH_3 background gas pressure was varied from 10^{-6}–10^{-3} Torr. The deposition rate and the film thickness were controlled by the pulse repetition rate (5–10 Hz) and total deposition time (30–60 min). With existing setup, uniform films (5% uniformity) can be grown up to a size of one inch diameter substrate. Upon utilizing laser and substrate scanning mechanisms, large area pusled laser deposition is feasible up to 3 to 4 inch substrates.

Heterostructures by Pulsed Laser Deposition

Two PLD chambers, one for oxides and the other for nitrides, evacuated by turbomolecular pumps to a base pressure of 1×10^{-7} Torr were used for fabrication of heterostructures. A KrF pulsed excimer laser was used for ablation of polycrystalline, stoichiometric

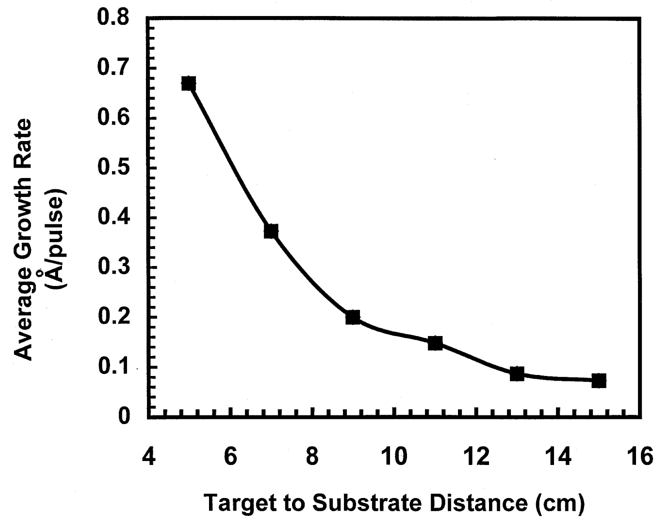

Fig. 2. The average growth rate of the AlN in PLD as a function of the distance (d) between the target and the substrate.

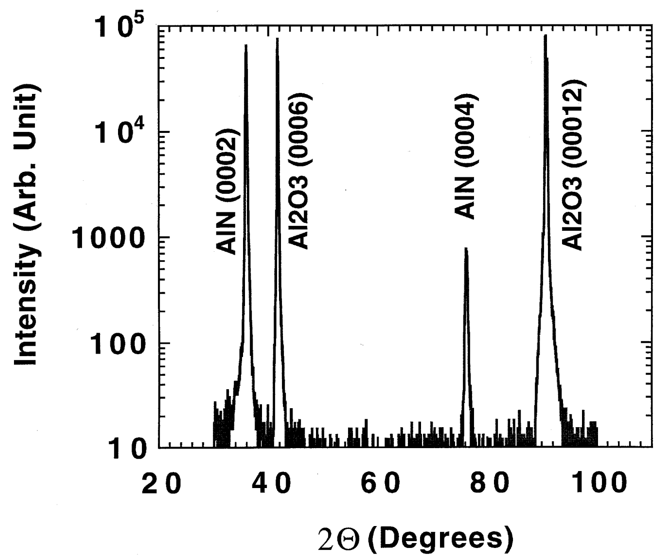

Fig. 3. XRD pattern of the epitaxial AlN thin film grown on sapphire (0001) substrate by PLD.

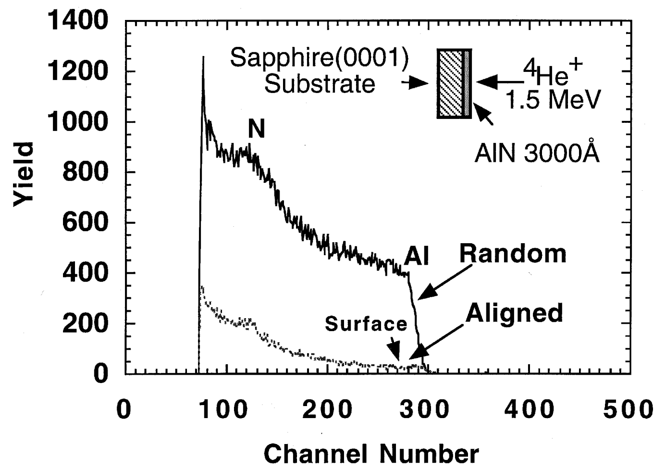

Fig. 4. Random and aligned Rutherford backscattering spectra of the epitaxial AlN film grown on sapphire (0001).

TiN and ZnO targets (99.99 purity). The laser energy density used for ablation of ZnO was ~1 J/cm^2, whereas for TiN, it was ~4–5J/cm^2. The average growth rate per pulse was found to be dependent on the substrate temperature, ambient pressure, and the distance between the target and the substrate and the details are reported later in the text. High quality epitaxial GaN buffer layers on sapphire (0001) substrates grown by either PLD or MOCVD were used for the fabrication of ZnO/GaN heterostructures. The ZnO films were grown at a substrate temperature ranging from 500 to 750°C and an oxygen partial pressure of 10^{-5}–10^{-4} Torr. To avoid the oxidation of the GaN surface, the initial deposition of ZnO up to a thickness of about 20Å was carried out at a reduced oxygen pressure (10^{-6} Torr).

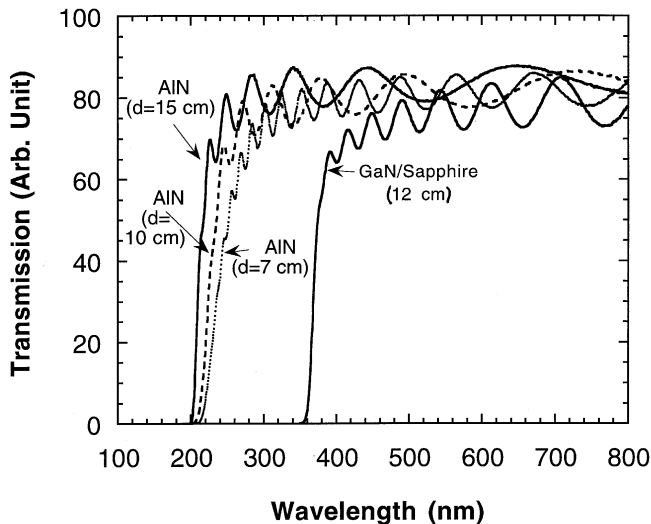

Fig. 5. Room temperature UV-visible optical transmission spectra of the AlN and GaN films grown at various target-to-substrate distances (d).

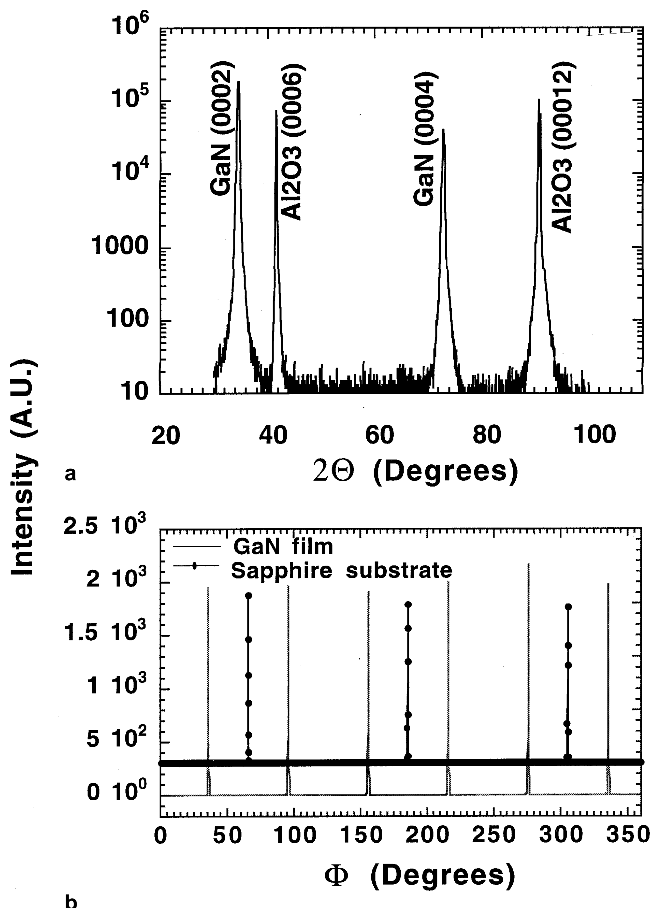

Fig. 6. (a) XRD Θ–2Θ pattern of the epitaxial GaN film grown by PLD on sapphire without buffer layer. (b) XRD ϕ scans for GaN{1011} peaks for a ~0.5 μm thick GaN film grown on sapphire (0001). In the ϕ scans, substrate peaks {1014} clearly indicate a 30° in-plane rotation of the film with respect to the sapphire substrate.

Characterization

The PLD films were characterized by four-circle x-ray diffraction (XRD), atomic force microscopy (AFM), UV-visible spectroscopy, photoluminescence spectroscopy (PL), low temperature cathodoluminescence spectroscopy (CL), and electrical transport measurements. The quantitative analysis of the crystalline quality, composition, and interface structure of the GaN films was determined by Rutherford backscattering spectrometry (RBS) and ion channeling techniques using a well collimated (divergence <0.01°) beam of 1.5–3 MeV He^+ ions. The atomic structure and interfaces of the heterostructures were characterized by high resolution transmission electron microscopy (HRTEM). The cross-section samples were prepared using a tripod polisher and ion milling. Transmission electron microscopy was conducted using a JEOL 4000FX transmission electron microscope operated at 300 kV. The high resolution images were obtained at a magnification of 400,000X.

RESULTS AND DISCUSSION

Pulsed Laser Deposition of AlN

The crucial parameters in the PLD of epitaxial films are the deposition temperature, background gas pressure, target to substrate distance, laser fluence, and pulse repetition rate. We have studied the dependence of these parameters on the crystalline quality, surface morphology, and optical and electrical properties of the III-V nitride films. We found that GaN and AlN grew epitaxially on sapphire (0001) at substrate temperature as low as 600°C. However, the crystalline quality of these films improved with an increase in the substrate temperature and the distance between the target and the substrate. High quality epitaxy was obtained when the films were grown under a background NH_3 gas pressure of -10^{-5} Torr and a substrate temperature of 750–850°C.

The dependence of the deposition rate on the distance between the target and the substrate was studied in the case of AlN thin film growth and the results are shown in Fig. 2. The growth rate falls with the relation $1/r^2$, where r is the distance between the target and the substrate. Above the critical distance of 9 cm, the crystallinity, surface morphology, and optical properties of the AlN films were found to be improved significantly. Figure 3 shows an XRD Θ–2Θ

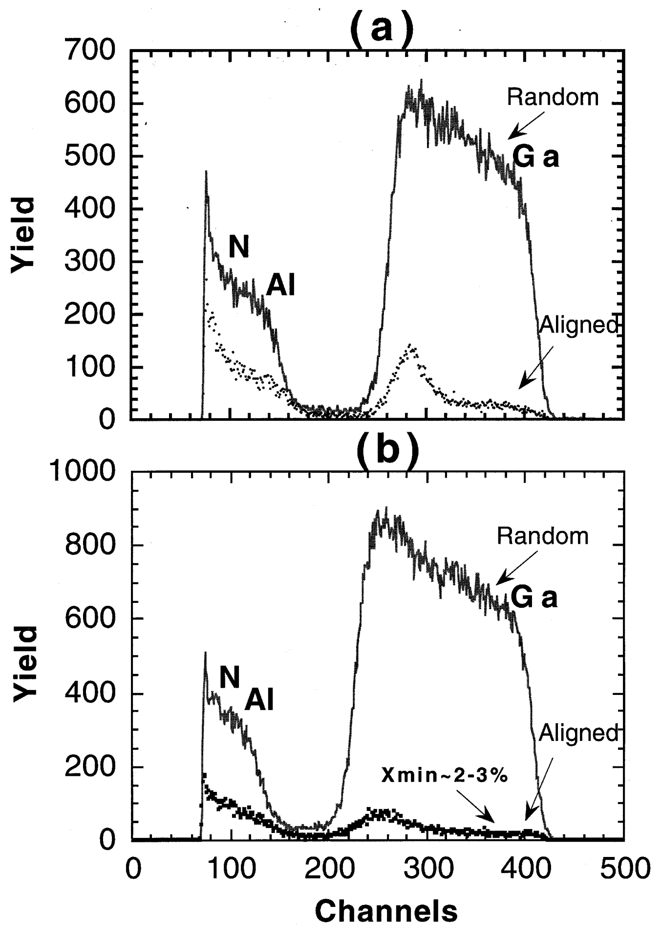

Fig. 7. Random and aligned Rutherford backscattering spectra for the GaN films grown (a) directly on sapphire (0001); and (b) with AlN buffer layer on sapphire (0001).

angular scan of a 2000Å thick AlN film grown at 850°C and the target-substrate distance of 15 cm. The XRD pattern clearly shows only a {0001} family of planes of wurtzite-AlN and sapphire indicating a high degree of texturing along the [0001] normal to the substrate. The FWHM of the XRD rocking curve (ω) for the (0002) AlN peak was found to be 7 arc min indicating an excellent alignment of (0001) lattice planes with that of sapphire (0001).

The quantitative analysis of the crystalline quality, composition, and interface structure of the III-V nitride films was carried out by RBS and ion channeling techniques using a well collimated (divergence <0.01°) beam of 1.5 MeV He^+ ions. The ratio of the RBS yield with the He^+ beam incident along [0001] (channeled) to that of a random direction, respectively, (χ_{min}), reflects the epitaxial quality of the film. Figure 4 shows the aligned and random backscattering spectra for the epitaxial AlN film grown on sapphire (0001). The minimum yield near the surface region of the films is ~3% indicating a high degree of crystallinity. These minimum yields are comparable to that of bulk single crystals. It should be noted that there always exist dislocations close to the interface due to a large lattice mismatch between the film and the substrate. Our channeling results shown in Fig. 4 (aligned spectra) clearly indicate an increase of the minimum yield up to ~10–12% near the interface region suggesting the presence of dislocations near the interface. These results are consistent with the transmission electron microscopic studies of the PLD[23] and CVD[3] films reported earlier.

Figure 5 shows the room temperature optical transmission spectra for the PLD AlN films grown at various target-to-substrate distances. The films displayed ~80–85% optical transmission in the near-visible optical range. A sharp absorption edge at 6.2 eV can be accurately determined for the high quality films by a linear fit of the square of the absorption coefficient as a function of the photon energy near the band gap. The band gap was found to be lower for the films grown at a shorter distance.

Pulsed Laser Deposition of GaN

Figure 6a shows the x-ray diffraction Θ–2Θ angular scans for ~5000Å thick GaN film grown by PLD. The x-ray diffraction results clearly show highly c-axis oriented films. The x-ray rocking curves were obtained to investigate the distribution of the crystals with definite orientation (mosaicity). Their alignment with respect to the substrate normal reflected in the FWHM of the rocking curve provides a measure of the epitaxial quality of the films. The FWHM for GaN film was less than 5 arc-min, and the K_α and K_β lines were clearly resolved in the XRD scans, indicating the high crystallinity of these films. Note that the film thickness in our case is lower than that of CVD films, and no intentional buffer layer was used. The degree of in-plane alignment was also determined using ϕ scans of $\{10\bar{1}1\}$ peaks with the ϕ rotation axis parallel to the c-axis of the film (Fig 6b). The in-plane epitaxial relationship was found to be GaN [1100] || sapphire $[12\bar{1}0]$. The FWHM of the GaN$(10\bar{1}1)$ peak observed in the ϕ scan was 0.55°.

The RBS spectra with He^+ ions incident along

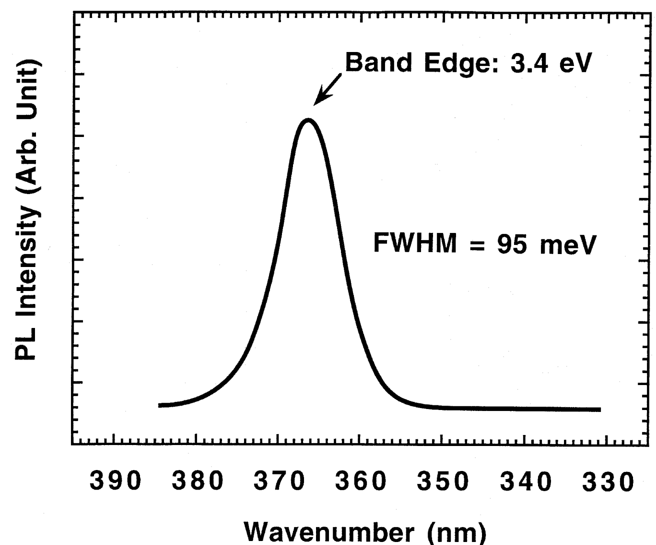

Fig. 8. Room temperature PL spectrum of GaN film grown on sapphire with AlN buffer by PLD.

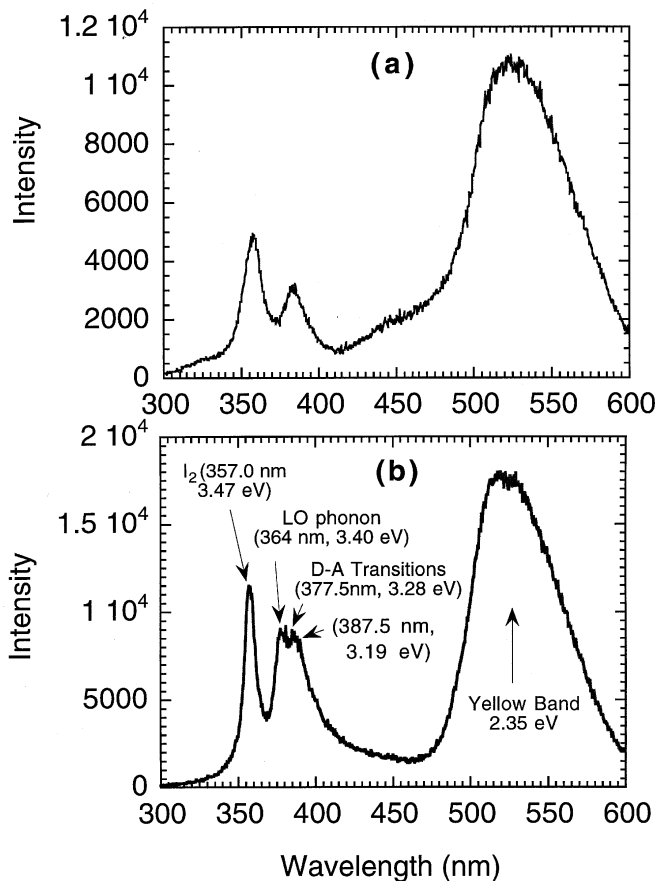

Fig. 9. Low temperature (8K) CL spectra of the PLD GaN films grown on (a) directly on sapphire, and (b) with AlN buffer layer.

random and channeling directions for the GaN film grown on sapphire with and without an AlN buffer layer are shown in Figs. 7a and 7b, respectively. From the ion channeling results, it is clear that the crystalline quality of the GaN near the surface and interface improved in the case of the AlN buffer layer. In the case of GaN/sapphire, a relatively high χ_{min} ~15–18% near the film-substrate interface is attributed to the formation of dislocations and low angle grain boundaries due to a large lattice mismatch (~16%) between the film and the substrate. The defect density at the interface is reduced in the case of the AlN buffer layer as shown in Fig 7b. The RBS spectra have also provided reasonable estimates of the composition and thickness of the films. The film thickness was determined using a computer fitting program, where the thickness is iteratively adjusted until the theoretical curve matched the experimental plot. The compositional analysis carried out for the GaN/Al_2O_3 interface showed the formation of a thin (~500Å) AlGaN layer. Such a layer could be formed because of the substrate exposure to NH_3 prior to deposition and its subsequent reaction with the ablated Ga. We have also found an excess of Ga in the films prepared at low substrate temperatures indicating that a limited amount of activated N was available due to the poor thermal decomposition of NH_3. From our experimental studies, the deposition process for GaN films using

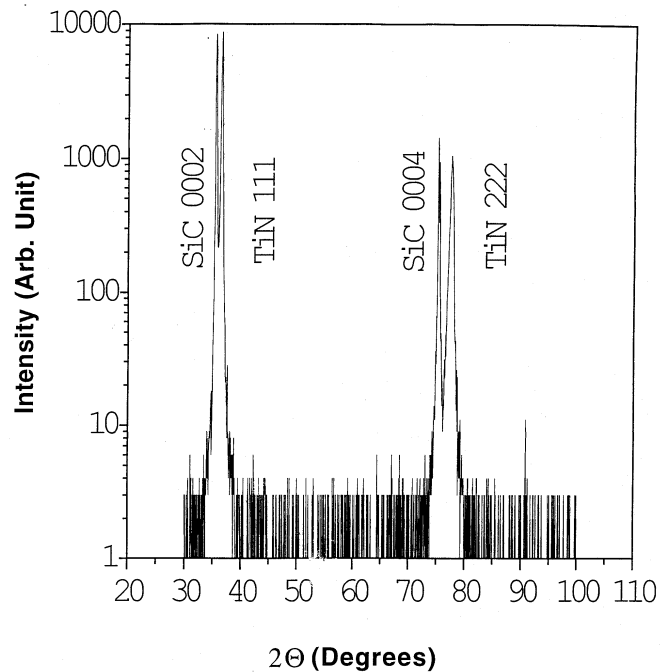

Fig. 10. XRD θ–2θ scan of an epitaxial TiN film deposited on SiC (0001) at 650°C.

NH_3 as a background gas appears to consist of two stages:

- The arrival of the laser ablated energetic species such as GaN, $GaN_{(1-x)}$, and Ga onto the heated sapphire substrate, and
- The epitaxial growth of GaN.[26]

In the second stage, if there is an excess of Ga during the growth, it could be either desorbed from the surface or trapped in the growing film depending on the substrate temperature and NH_3 pressure. The analysis of the RBS spectra clearly shows an excess of Ga in the films grown at ~600°C. At higher temperatures, the film composition was close to that of the stoichiometric GaN suggesting either desorption of the excess Ga or formation of GaN due to a stronger activation of NH_3 at the higher substrate temperature. The desorption of Ga was reflected in a decrease of the GaN growth rate when the substrate temperature was increased.

Figure 8 shows the room temperature photoluminescence spectrum of the epitaxial GaN films grown on sapphire with an AlN buffer layer. A band edge emission is observed for PLD GaN films at 3.4 eV. Figures 9a and 9b show the low temperature cathodoluminescence (CL) spectra of the epitaxial GaN films grown on sapphire with and without the AlN buffer layer, respectively. These spectra clearly show the emission lines due to the recombination of excitons bound to neutral donors (called I_2 line), transitions from donor-acceptor impurities and the well known yellow band. From our RBS ion channeling studies discussed earlier, it is clear that the films grown on the AlN buffer layer have fewer structural defects than the films grown directly on the sapphire substrate. From the CL results, it is seen that the

ratio of the exciton emission peak to the D-A transition peak is enhanced in the case of the AlN buffer layer. These results clearly indicate that the structural defects present in the GaN films grown on sapphire without a buffer layer are responsible for the poor optical properties of these GaN films.

The films grown at 750°C were shiny, and the surface roughness as measured by AFM for the GaN film grown on sapphire and AlN/sapphire was ~20 and 5–8 nm, respectively. The electrical resistivity at room temperature for ~0.5 μm thick film was $\sim 10^{-2}$–10^{3} Ω-cm, the mobility was 25–60 $cm^2V^{-1}s^{-1}$, and the carrier concentration was 5×10^{15}–6×10^{19} cm^{-3}.

Epitaxial TiN Ohmic Metallization of GaN and SiC by PLD

In order to operate the III-V nitride and SiC based devices at high temperature and high power conditions, reliable and low resistance ohmic contacts are necessary for the devices since maximum speed and high-power performance depend critically on the contact resistances. Generally, a metal with an optimal barrier height is chosen along with a degenerate surface layer created by ion implantation. However, very little flexibility is available in SiC because its Fermi level is pinned at the surface.[27,28] In practice, forming ohmic contacts by heavy impurity doping is rather difficult in the case of SiC. A high temperature exceeding 1800°C is required[29] to facilitate thermal diffusion in order to form a heavily doped SiC layer with a carrier concentration of 10^{18} cm^{-3}. In the case of GaN, low temperature annealing is good enough to form the low resistance contacts. First investigation of n-type GaN contacts by Foresi and Moustakas[30] reported on the resistivity of 10^{-4} Ωcm^2 and 10^{-3} Ωcm^2 achieved using Al and Au metallizations, respectively. Khan et al. used Ti/Au to produce a contact resistivity of 7.8×10^{-4} Ωcm^2 on n-type GaN.[31] Ti/Al metallization helped Morkoç et al. to achieve a contact resistivity to n-type GaN (10^{17} cm^{-3}) of 8×10^{-6} Ωcm^2 after a 30 s rapid thermal anneal at 900°C.[32] The most likely mechanism for the low contact resistance is solid phase epitaxy of TiN_x via N out-diffusion from GaN. Two monolayers of TiN formed at the interface are sufficient to create a 10 nm thick surface layer of GaN featuring a carrier density of 10^{20} cm^{-3} through which charge carriers could efficiently tunnel.

In this context, we have developed a novel approach that utilizes epitaxial TiN layers to obtain ohmic contacts to SiC and GaN.[33] Since the contact properties are affected by the height of the Schottky barrier present at the interface to a higher degree than by the work function of the contact metal, Fermi level pinning must be suppressed to lower the barrier height.[34] The pinning is dependent on the interface state density, which can be lower at epitaxial interfaces; a greatly reduced number of structural defects and grain boundaries in the case of epitaxial contacts may result in a larger effective area of the contact and a decreased resistivity of the contact material.

Thin TiN films were grown on 6H-SiC and GaN/sapphire for contact resistance measurements using PLD. The films deposited at substrate temperatures in the range from 200 to 550°C were essentially polycrystalline and consisted of fine grains of TiN oriented along the [111] direction normal to the SiC (0002) plane of the substrate. The TiN films grew epitaxially at substrate temperatures above 550°C. The results of an XRD θ–2θ angular scan of a 200 nm thick TiN film deposited on SiC (0001) at 650°C are shown in Fig. 10. These results clearly show that the {111} family of planes of TiN are aligned parallel to the (0002) planes of the SiC substrate. The rocking curve FWHM of the TiN (111) peak for a film grown at 650°C was about 0.35°, indicating a good alignment of the TiN (111) lattice planes with the SiC (0001). Similar results were obtained in the case of TiN epitaxy on GaN (0001). This type of epitaxial relationship is expected since TiN has a cubic structure with a = 4.24Å, and the interplanar distance between the TiN (111) planes is about 3.0Å which is close to the hexagonal 6H-SiC lattice constant, 3.08Å. Under this relationship, the lattice misfits between TiN/SiC and TiN/GaN are 2.6 and 3.0%, respectively, which are low enough to achieve epitaxial growth of TiN on SiC and GaN.

To investigate the contact properties of TiN and their dependence on the film's crystallinity, 200 nm thick TiN films were deposited at 20, 400, 600, and 800°C on 6H-SiC and GaN/sapphire substrates loaded simultaneously. The TiN films on all samples were consequently patterned into an array of 4×12 mm^2 Schockley pads involving photolithography and ion milling. The contact resistivity measurements of TiN/SiC and TiN/GaN interfaces were conducted using the transmission line method (TLM) with a constant 10 V bias sequentially applied between various pairs of the pads. The plots of contact resistivity of TiN vs TiN deposition temperature are displayed in Fig. 11 for n-type 6H-SiC and GaN samples with nominal

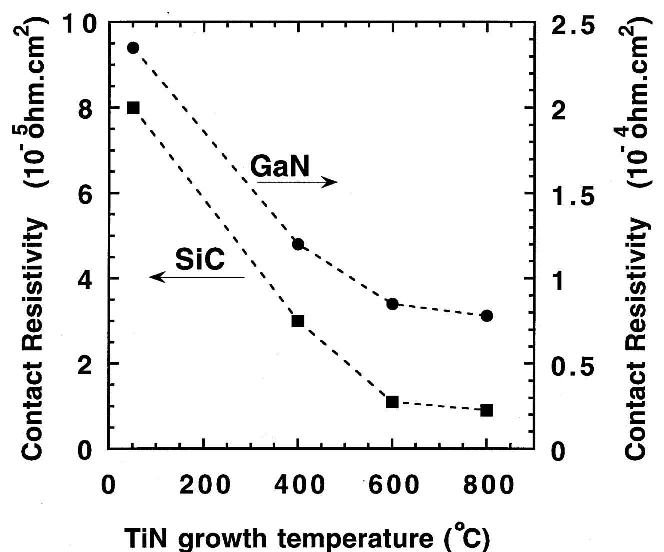

Fig. 11. Plots of contact resistivity of TiN to n-type 6H-SiC (squares) and GaN (circles) vs TiN deposition temperature.

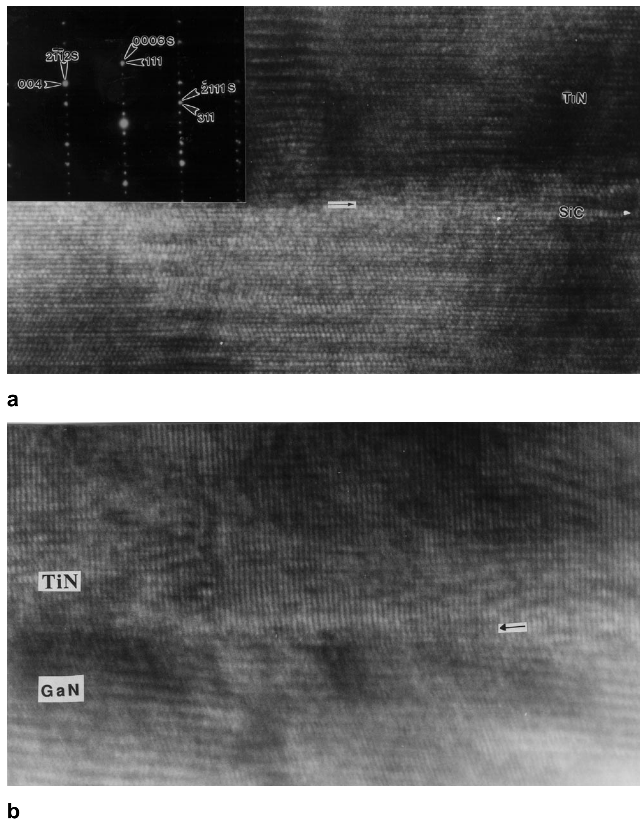

Fig. 12. HRTEM lattice images of (a) TiN/SiC and (b) TiN/GaN interfaces.

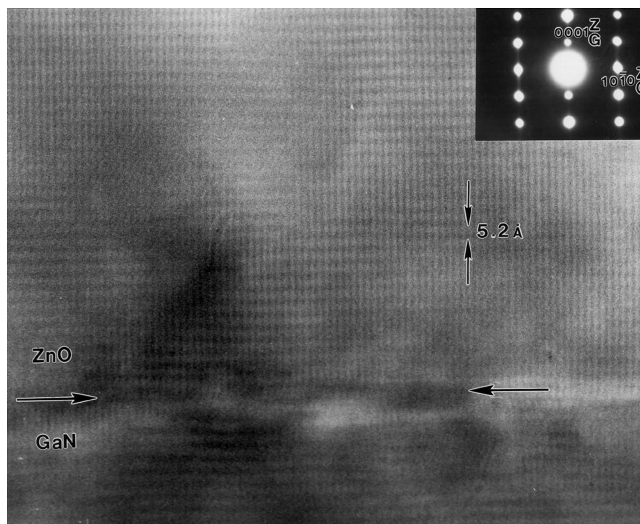

Fig. 13. HRTEM lattice image and the corresponding selective area electron diffraction pattern of the ZnO/GaN interface.

carrier concentration densities of 3.7×10^{18} cm^{-3} and 4.6×10^{16} cm^{-3}, respectively. Both plots exhibit a sharp drop of the contact resistivity as the TiN deposition temperature increases producing a more crystalline material. The substrate temperature of 600°C is known to be the lower temperature limit for growing TiN films of reasonable crystallinity. In agreement with our expectations, the contact resistance value for TiN deposited at 600°C differs from that for the 400°C sample more drastically than from the contact resistance value of the TiN grown at 800°C, since the degree of TiN crystallinity is not changing as much between 600 and 800°C as it does between 400 and 600°C. The contact resistivity values for the epitaxial TiN/SiC and TiN/GaN samples were measured to be 1.1×10^{-5} Ωcm^2 and 7.9×10^{-5} Ωcm^2, respectively, which are in the lowest range reported. To understand the interface between the metal and semiconductors, high resolution transmission electron microscopy was used and the TEM images are shown in Fig. 12. The TEM results show that the TiN grown on SiC and GaN is highly crystalline with twined structures. Although the substrate/interface is not perfectly smooth, it is abrupt and we see no sign of interdiffusion. This indicates that the flatness deviations are a characteristic of this particular substrate rather than a result of film growth. The TiN/GaN/sapphire sample also has abrupt interfaces with no indication of interdiffusion. The (111) dark field image shows that the film is well oriented along the (111) growth direction constant with the x-ray diffraction studies. Thus, the clean interface with fewer defects may be responsible for the low resistance ohmic contacts to the GaN and SiC.

Metal-Oxide/GaN Heterostructures by PL D

Another material analogous to GaN is ZnO which has a room temperature band gap of 3.3 eV and the wurtzite structure with lattice constants of a = 3.18Å and c = 5.24Å. It is also being considered as a promising material for UV and blue light emitting devices.[35–40] The interesting features of ZnO are:

- A large exciton binding energy[2] (60 meV) which may be useful for efficient UV laser applications based on stimulated emission due to the recombination of excitons at room temperature (kT = 24 meV),
- Low power thresholds for optical pumping at room temperature,[36] and
- Tunable band gap from 2.8 to 3.3 eV and 3.3 to 4 eV by alloying with CdO and MgO, respectively.[37]

The optically pumped lasing in the ZnO bulk crystals was studied by Hvam et al.[38] and more recently by Reynolds et al.[36] Room temperature optically pumped lasing in epitaxial ZnO films grown on sapphire (0001) was demonstrated recently by groups of Kawasaki and Koinuma,[39] and Bagnall et al.[40]

We have studied the ZnO epitaxy on high quality GaN buffer layers on sapphire (0001). The ZnO films grown on epi-GaN/sapphire were found to be single crystalline due to the match of stacking order and a low lattice misfit (1.9%) between GaN and ZnO as compared to those grown directly on sapphire. The x-ray diffraction measurements showed highly c-axis oriented films with a rocking curve FWHM of 3 arc-min. The *in-plane* epitaxial relationship in these heterostructures was found to be ZnO[1010]||GaN[1010] || Al_2O_3 [1120]. The FWHM of the (1011) peak for both ZnO and GaN was about 15 arc-min, and no tilting was observed between the ZnO and GaN films. These measurements indicate that

this misorientation is much smaller than that for ZnO epilayers grown directly on sapphire (0001).[22]

The ion channeling measurements on these films showed a minimum yield near the surface region of ~1–2%. The dechanneling analysis shows that the dislocation densities near the ZnO/GaN and ZnO/sapphire interfaces are $2 \times 10^3/cm^2$ and $4 \times 10^9/cm^2$, respectively. Figure 13 shows the HRTEM lattice image and selective area electron diffraction (SAED) pattern of ZnO/GaN interface. These results show that the lattice planes of ZnO are perfectly aligned with those of GaN and the interface is fairly sharp. These results confirm the suitability of a GaN buffer layer for ZnO growth. Figure 14 shows a CL spectrum obtained at 8K for a 5000Å ZnO epilayer grown on epi-GaN/sapphire. The CL spectra for the ZnO film on GaN/sapphire demonstrate distinct peaks due to the free A-exciton and D°X bound exciton. In addition to this, the CL spectra show pronounced features due to the donor-acceptor pair transitions at 3.32 eV with phonon replicas at 3.25 and 3.18 eV. From the CL studies, we also note the FWHM of a free A-exciton line width is about 20 meV which is comparable to that of device quality GaN films. The intense CL peak and the absence of a green band clearly indicate the high quality epitaxy of ZnO on GaN/sapphire.

We also compare the thermally induced strain and its effect on the optical properties of the ZnO/GaN epilayers on sapphire. Both ZnO and GaN films on sapphire are under compressive strain. The thermal mismatch for ZnO on sapphire is 13.2% which is smaller than that for GaN/sapphire (25.5%). Thus, the relatively small values of thermal and lattice strains for ZnO films on GaN/sapphire imply that the ZnO films are under reduced strain. Our CL studies reveal that the free and bound exciton transitions in the case of the ZnO/GaN/sapphire sample are close to those of a bulk ZnO crystal.

Due to their lattice matching epitaxy and thermal and optical compatibility, the ZnO/GaN heterostructures on sapphire may be useful for fabrication of hybrid optoelectronic devices exploiting advantages of both ZnO and GaN. Recently, Hamdani et al.[42] have demonstrated high optical quality epitaxial GaN films on ZnO crystals by molecular beam epitaxy (MBE). It means that under MBE and PLD growth conditions, high quality ZnO/GaN and GaN/ZnO heterostructures can be integrated on sapphire. Another interesting feature of a thick GaN buffer layer for ZnO is its high thermal conductivity which may be beneficial for ZnO thin film lasers. At this juncture, we feel optimistic about the possibility of being able to fabricate novel p-n junctions based on n-type ZnO (Al or Ga doped) and p-type GaN (Mg-doped) semiconductors for light emitting devices. The doped films can be grown by using doped targets. The high electrical conductivity and optical transparency achieved in doped ZnO epilayers may also be utilized as the transparent electrodes for blue GaN optical devices.

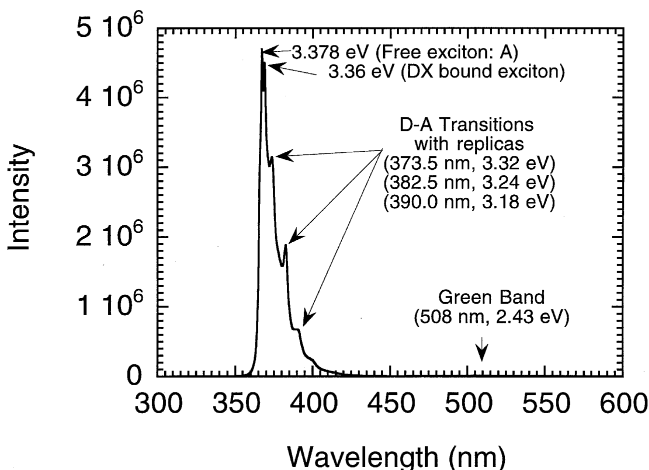

Fig. 14. Low temperature (8K) CL spectrum for a 0.5 μm thick epitaxial ZnO film grown on epiGaN/sapphire substrate.

Pulsed Laser Etching of GaN and AlN Nitrides

To fully realize the device potential of these materials, various etching techniques involving wet and dry processing needs to be established. Since GaAlN strongly resists wet chemical etchants due to its high bond energies, dry etching processes are becoming more relevant for device fabrication of III-V nitrides.

Various dry etching techniques have been vigorously pursued in the interest of effective device processing.[2] These include reactive ion etching (RIE),[43] plasma etching,[44] chemically assisted reactive ion beam (RIB) etching,[45] and ECR etching.[46] To date, the highest etch rates for GaN are 4700Å/min by RIE,[47] and 2850Å/min by ECR plasma etching at room temperature.[48] Typically, chemically assisted RIB tends to cause more damage to the material than ECR because it has a higher ion energy. Here we report another dry processing technique, pulsed laser etching, that can be utilized for the controlled etching of GaN and AlN heterostructures. In the past, this technique has been successfully employed for dry etching of metal-oxide films.[49,50] Recently, a similar approach was demonstrated in the etching and patterning of GaN films using a Nd:YAG laser operating at a wavelength of 355 nm, and etch rates of 500–700Å per pulse were obtained.[51]

In our case, we have studied pulsed laser etching of GaN and AlN films using a KrF excimer laser operating at 248 nm with a pulse duration of 30 ns. In the etching experiments, a uniform portion of a KrF excimer laser beam was selected by a 15 mm × 7 mm thin metal aperture and subsequently focused on the samples by a lens of 25 cm focal length. The GaN film was mounted perpendicular to the laser beam behind the focal point and shielded by a copper plate resting against its surface. A rectangular array of circular holes (250 mm in diameter) were drilled in the copper plate, so that only the surface exposed under the holes was etched. This arrangement produced several (8–10) identical etch patterns each time the film was laser etched. A wide range of incident energy fluences (0.2 to 10 J/cm^2) was explored for etching the GaN and AlN films. It was achieved by varying either the

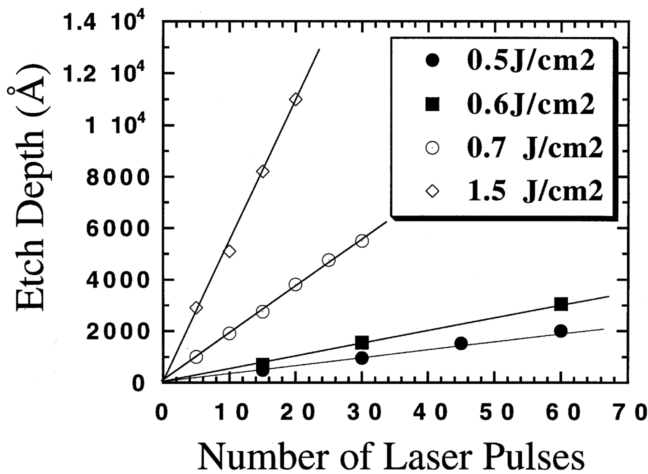

Fig. 15. The dependence of etch rate on the number of laser pulses at various energy densities indicated in the inset.

distance between the sample surface and the lens or the output energy of the laser. The etching was carried out in air at room temperature. After the laser etching experiments, the samples were cleaned in dilute HCl to remove a thin layer of Ga that was formed due to the thermal decomposition of GaN by the laser beam. The etch depth was measured using a mechanical stylus.

First, we studied the dependence of the etch depth on the number of laser pulses at various energy densities. The etch depth was found to increase linearly with the number of pulses over a wide range of incident energy densities as shown in Fig. 15. The slope of each line demonstrates the etch rate of GaN. The dependence of the etch rate on the incident laser energy density is plotted in Fig. 16. The threshold incident energy density, below which no etching occurs, can be obtained from the plot by extrapolation, and it is found to be $E_{th} = 0.41$ J/cm². For a high quality epitaxial GaN film, a surface reflection of about 20% is measured at normal incidence.[52] Taking this into account, our measurements show E_{th} to be about 0.33 J/cm². Similar measurements were carried out on AlN thin films, and the threshold energy density is estimated to be 0.6 J/cm². At ~1 J/cm² the etch rate is about 320Å/pulse, whereas at 5 J/cm² it is about 1100Å/pulse. Since the etch rate depends linearly on the number of pulses, by operating the laser at few tens of Hz, etch rates of about 1 μm/s can be easily obtained in GaN. These are the highest etch rates among the reported values for GaN. We assume that the energy density inside the sample has a profile in the form of a Beer-Lambert type relationship as:

$$E(z) = E_{inc} \exp(-\alpha z) \quad (1)$$

where E(z) is the attenuated energy density at depth z below the surface of the GaN film, E_{inc} is th incident laser energy density, and α is the absorption coefficient (inverse of absorption length). To extract the absorption length and the linear absorption coefficient, the etch rate is plotted as a function of In (E) as shown in Fig. 17. For $E(z) = E_{th}$, we get:

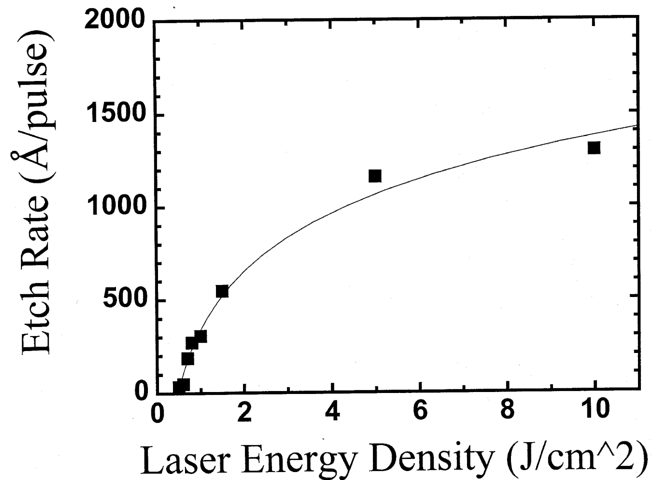

Fig. 16. Variation of etch rate as a function of incident laser energy density.

$$\text{etch depth/pulse} = 1/\alpha \ \mathrm{In}\ (E_{inc}/E_{th})$$
$$= 1/\alpha \ \mathrm{In}\ (E_{inc}) - 1/\alpha\ (E_{th})$$
$$E(z) = E_{inc} \exp(-\alpha z)$$

A plot of the etch rate vs In (E_{inc}) is linear with the slope d = 1/α, the absorption length. Our experimental results, as shown in Fig. 17, indicate the linear dependence of the etch rate on In(E). From the slope, we determined the absorption length to be 42 nm and the absorption coefficient to be 2.3×10^5 cm^{-1}. This value is consistent with the absorption coefficient of GaN reported elsewhere.[11] Figure 18 shows etch depth profiles obtained in the laser etching of GaN films at various energy densities. The original surface roughness of the GaN film is about few 10 nm. Three distinct features of the laser etch patterns are:

- The highly anisotropic etch profiles with sharp edges,
- Convex shape of the bottom of the etch obtained at low energy densities (below 1J/cm²), and
- Flat surface of the bottom of the etch above 1J/cm².

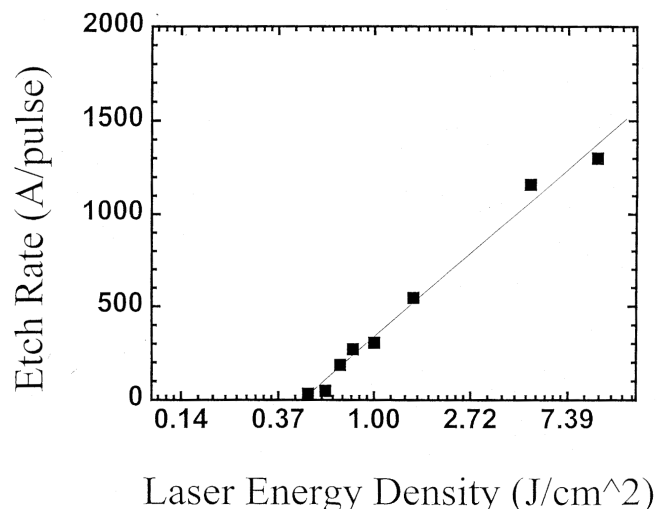

Fig. 17. Semilog plot of the etch rate as a function of laser energy density.

The convex shape of the bottom may be due to two reasons:

- The material that is etched during laser processing partially screens the central portion of the incident laser beam, thereby damping the etching in the center of the region; and
- Some of the ablated material redeposits onto the etched area, forming a hump in the center.

The same type of profile and the contributing effects have previously been observed in the laser etching of high-T_c superconducting thin films.[49] Since the dominant mechanism for laser etching of GaN is identified as the thermal decomposition and the forward ejection with nitrogen effusion, only residual Ga is expected to redeposit in the hump area in the etched region. However, after chemical etching in dilute HCl, we did not see any significant change in the profile near the bottom surface. This clearly indicates shielding of the laser beam by the ablated species at the low energy density regime. As the energy density increases above 1J/cm^2, a relatively flat bottom of the etched region is achieved. This indicates that the etching mechanism is based on highly forward directed ejection of the material and it increases with the equilibrium laser energy density in comparison with the laser evaporation process which occurs at lower energy densities.

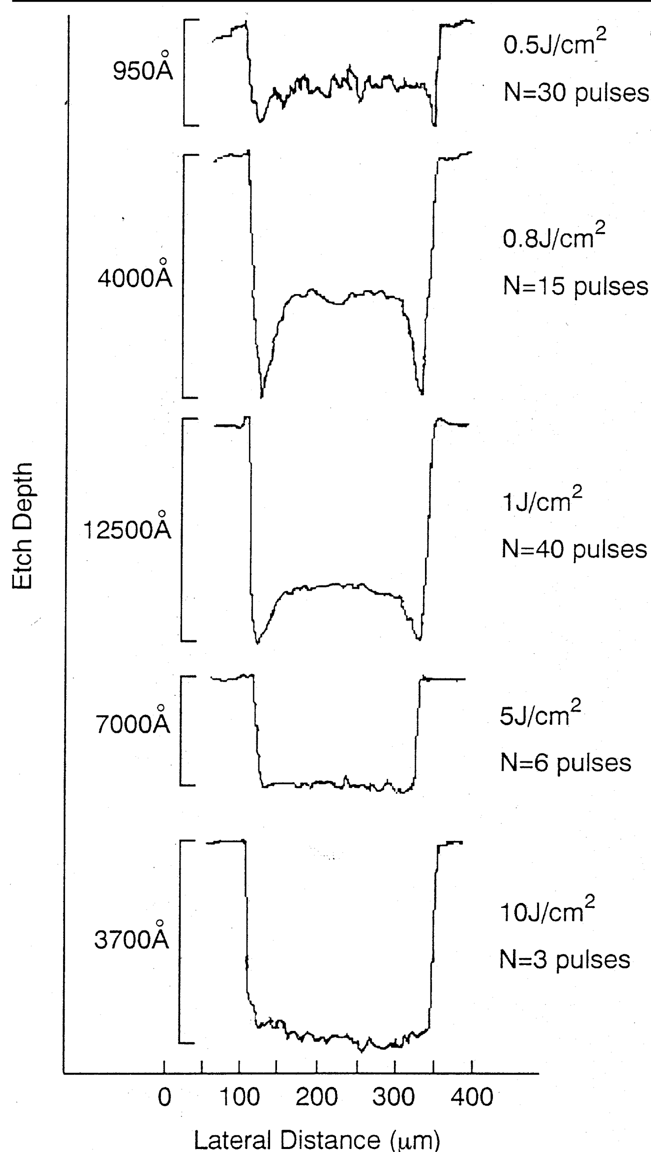

Fig. 18. Etch profiles obtained after GaN etching by laser pulses at various number of pulses and laser energy densities: (a) 30 pulses with 0.5 J/cm^2, (b)15 pulses with 0.8 J/cm^2, (c) 40 pulses with 1 J/cm^2, (d) 6 pulses with 5 J/cm^2, and (e) 3 pulses with 10 J/cm^2.

CONCLUSION

We have developed the pulsed laser deposition technique for the growth of high crystalline quality epitaxial thin films of III-V nitrides, semiconducting ZnO, and metallic TiN. The epitaxial quality and optical properties of GaN and AlN were found to be strongly dependent on the laser fluence, substrate temperature, substrate to target distance, and background gas pressure. The GaN and AlN films grown on sapphire (0001) showed FWHM of the rocking curve of 5–7 arc-min with an in-plane misorientation of ~0.5°, and an ion channeling minimum yield of ~3–5%. The capability of PLD for the fabrication of heterostructures of nitride/nitride (GaN/AlN and TiN/GaN), nitride/carbide (AlN/SiC, TiN/SiC), and oxide/nitride (ZnO/GaN) has been demonstrated. The HRTEM studies revealed sharp interfaces between nitride-nitride, nitride-silicon carbide, and oxide-nitride heterostructures. Epitaxy of TiN and its low contact resistance on SiC and GaN are useful for high temperature and high power devices. Our research demonstrates that the PLD technique may play an unique role for the integration of advanced materials based on III-V nitrides, metal oxides, carbides, and fabrication of their heterostructures for novel device applications.

ACKNOWLEDGMENTS

We thank Dr. Ogale, Adam Balsomo, and Jothi Narayanan of the University of Maryland at College Park, and M. He, X. Tang, J.B. Halpern, and M.G. Spencer of Materials Science Research Center of Excellence, Howard University, DC, for helpful discussion. This work was supported with an MRCP Army Grant, DAAL019523530.

REFERENCES

1. For a review, see S. Nakamura and G. Fasol, *The Blue Laser Diode* (Berlin: Springer, 1997), and also S. Strite and H. Morkoç, *J. Vac. Sci. Technol. B* 10, 1237 (1992); H. Morkoç, S. Strite, G.B. Gao, M.E. Lin, B. Sverdlov and M. Burns, *J. Appl. Phys*. 76, 1363 (1994); and references therein.
2. "GaN and Related Materials for Device Applications," *Mater. Res. Soc. Bulletin* 22, (1997), and references therein.
3. W. Qian, M. Skowronski, M. De Graef, K. Doverspike, L.B. Rowland,and D.K. Gaskill, *Appl. Phys. Lett*. 66, 1252 (1995).
4. J.N. Kuznia, M.A. Khan, D.T. Olson, R. Kaplan and J. Freitas, *J. Appl. Phys* 73, 4700 (1993).
5. S. Yoshida, S. Misawa and S. Gonda, *Appl. Phys. Lett*. 42, 427 (1983).
6. O.H. Nam, M.D. Bremser, T. Zheleva and R.F. Davis, *Appl. Phys. Lett.* 71, 2638 (1997).

7. S. Nakamura, M. Senoh, S. Nagahama, N. Iwasa, T. Yamada, T. Matsushita, H. Kiyoku, Y. Sugimoto, T. Kozaki, H. Umemoto, M. Sano and K. Chocho, *Jpn. J. Appl. Phys*. 37, L309 (1998).
8. S. Nakamura, Y. Harada and M. Seno, *Appl. Phys. Lett*. 58, 2021 (1991).
9. P. Kung, A. Saxler, X. Zhang, D. Walker, T.C. Wang, I. Ferguson and M. Razeghi, *Appl. Phys. Lett.* 66, 2958 (1995).
10. M.A. Khan, R.A. Skogman, J.M. Van Hove, D.T. Olson and J.N. Kuznia, *Appl. Phys. Lett.* 60, 1366 (1992).
11. N.H. Karam, T. Parodos, P. Colter, D. McNulty, W. Rowland, J. Schetzina, N. El-Masry and S.M. Bedair, *Appl. Phys. Lett.* 67, 94 (1995).
12. I. Akasaki, H. Amano, H. Murakami, M. Sassa, H. Kato and K. Manabe, *J. Cryst. Growth* 128, 379 (1993).
13. W. Qian, M. Skowronski, M.D. Graef, K. Doverspike, L.B. Rowland and D.K. Gaskill, *Appl. Phys. Lett.* 66, 1252 (1995).
14. R.J. Molnar, R. Singh and T.D. Moustakas, *Appl. Phys. Lett*. 66, 268 (1995).
15. W. Kim, O. Aktas, A.E. Botchkarev, A. Salvador, S.N. Mohammad and H. Morkoç, *J. Appl. Phys. Lett*. 79, 7657 (1996).
16. R.C. Powell, N.-E. Lee, Y.-W. Kim and J.E. Greene, *J. Appl. Phys.* 73, 189 (1993).
17. Z. Yang, L.K. Li and W.I. Wang, *Appl. Phys. Lett*. 67, 1686 (1995).
18. M.J. Paisley and R.F. Davis, *J. Cryst. Growth* 162, 537 (1990).
19. R.D. Vispute, V. Talyansky, R.P. Sharma, S. Choopun, M. Downes, T. Venkatesan, K.A. Jones and A.A. Iliadis, Fourth Intl. Conf. on Laser Ablation, Monterey, CA, July 21–25, 1997; *Appl. Surf. Sci.* 127-129, 431 (1998).
20. R.D. Vispute, V. Talyansky, S. Choopun, M. Downes, R.P. Sharma and T. Venkatesan, M.C. Wood, R. T. Lareau, K.A. Jones and A.A. Iliadis, *Appl. Phys. Lett*. 71, 102 (1997).
21. *Pulsed laser deposition of thin films*, ed. D. Chrisey and G. Hubler, (New York: Wiley-Interscience, 1994), and references therein.
22. R.D. Vispute, V. Talyansky, S. Choopun, M. Downes, R.P. Sharma and T. Venkatesan, M.C. Wood, R.T. Lareau, K.A. Jones and A.A. Iliadis, *Appl. Phys. Lett.* 70, 2735 (1997).
23. R.D. Vispute, H. Wu and J. Narayan, *Appl. Phys. Lett*. 67, 1549 (1995).
24. R.F. Xiao, X.W. Sun, H.B. Liao, N. Cue and H.S. Kwok, *J. Appl. Phys.* 80, 4226 (1996).
25. T. Huang and J.S. Harris, Jr., *Appl. Phys. Lett*. 72, 1158 (1998).
26. P. Kung, C.J. Sun, A. Saxler, H. Ohsato and M. Razeghi, *J. Appl. Phys.* 75, 4517 (1994).
27. S. Hara, T, Teraji and K. Kajimura, *Appl. Surf. Sci.* 107, 218 (1996).
28. S.R. Smith, A.O. Evwaraye,and W.C. Mitchel, *J. Appl. Phys*. 79, 301 (1996).
29. J.A. Edmond, H.J. Kim and R.F. Davis, *Mater. Res. Soc. Proc*. 52, (Pittsburgh, PA: Mater. Res. Soc., 1986), p. 157.
30. J.S. Foresi and T.D. Moustakas, *Appl. Phys. Lett*. 62, 2859 (1993).
31. M.A. Khan, J.N. Kuznia, A.R. Bhattarai,and D.T. Olson, *Appl. Phys. Lett.* 62, 1786 (1993).
32. H. Morkoç, S. Strite, G.B. Gao, M.E. Lin, B. Sverdlov and M. Burnes, *J. Appl. Phys.* 76, 1363 (1994).
33. V. Talyansky, R.D. Vispute, S.N. Andronescu, A.A. Iliadis, K.A. Jones, S. Choopun, M.J. Downes, R.P. Sharma, T. Venkatesan, Y. X. Li, L.G. Salamanca-Riba, M.C. Wood and R.A. Lareau, *Mater. Res. Soc. Symp. Proc*., (Pittsburgh, PA: Mater. Res. Soc., 1997).
34. S.M. Sze, *Physics of Semiconductor Devices*, (New York: John Wiley and Sons, 1981).
35. J.M. Hvam, *Solid State Commun*. 26, 987 (1978).
36. D.C. Reynolds, D.C. Look, and B. Jogai, *Solid State Commun*. 99, 873 (1996).
37. A. Ohtomo, M. Kawasaki, T. Koida, H. Koinuma, Y. Sakurai, Y. Yoshida, M. Sumiya, S. Fuke, T. Yasuda and Y. Segawa, *Mater. Sci. Forum* 264 (2), 1463 (1998).
38. J.M. Hvam, *Solid State Commun*. 12, 95 (1973).
39. M. Kawasaki, A. Ohtomo, H. Koinuma, Y. Sakurai, Y. Yoshida, Z.K. Tang, P. Yu, G.K.L. Wang and Y. Segawa, *Mater. Sci. Forum* 264 (2), 1459 (1998).
40. D.M. Bagnall, Y.F. Chen, Z. Zhu, T. Yao, S. Koyama, M.Y. Shen and T. Goto, *Appl. Phys Lett*. 70, 2230 (1997).
41. R.D. Vispute, Talyansky, S. Choopun, R.P. Sharma and T. Venkatesan, M. He, X. Tang, J.B. Halpern and M.G. Spencer, Y.X. Li and L.G. Salamanca-Riba, A.A. Iliadis and K.A. Jones, *Appl. Phys. Lett.* 73, 348 (1998).
42. F. Hamdani, A. Botchkarev, W. Kim, H. Morkoç, M. Yeadon, J.M. Gibson, S.-C. Y. Tsen, D.J. Smith, D.C. Reynolds, D.C. Look, K. Evans, C.W. Litton, W.C. Mitchel and P. Hemenger, *Appl. Phys. Lett.* 70, 467 (1997).
43. M.E. Lin, Z.F. Fan, Z. Ma, L.H. Allen and H. Morkoç, *Appl. Phys. Lett.* 64, 887 (1994).
44. R.J. Shul, G.B. McClellan, S.A. Casalnuovo, D.J. Rieger, S.J. Pearton, C. Constantine, C. Barratt, R.F. Karlicek, C. Tran and M. Schurman, *Appl. Phys. Lett*. 69,1119 (1996).
45. A.T. Ping, I. Adesida and M. Asif Khan, *Appl. Phys. Lett*. 67,1250 (1995).
46. C.B. Vartuli, S.J. Pearton, J.W. Lee, J. Hong, J.D. MacKenzie, C.R. Abernathy and R.J. Shul, *Appl. Phys. Lett*. 69, 1426 (1996).
48. R.J. Shul, A.J. Howard, S.J. Pearton, C.R. Abernathy, C.B. Vartuli, P.A. Barnes and M.J. Bozack, *J. Vac. Sci. Technol. B* 13, 2016 (1995).
49. A. Inam, X.D. Wu, T. Venkatesan, S.B. Ogale, C.C Chang and D. Dijkkamp, *Appl. Phys. Lett*. 51,1112 (1987).
50. A.M. Dhote, R. Shreekala, S.I. Patil, S.B. Ogale, T. Venkatesan and C.M. Williams, *Appl. Phys. Lett*. 67, 3644 (1995).
51. M.K. Kelly, O. Ambacher, B. Dahlheimer, G. Groos, R. Dimitrov, H. Angerer and M. Stutzmann, *Appl. Phys. Lett.* 69, 1749 (1996).
52. S. Bloom, G. Hardeke, E. Meier and I.B. Ortenburger, *Phys. Status Solidi* 66,161 (1974).